

Dynamics of polymer electrolyte fuel cells undergoing load changes

Yun Wang, Chao-Yang Wang*

*Electrochemical Engine Center (ECEC), Department of Mechanical and Nuclear Engineering,
The Pennsylvania State University, University Park, PA 16802, USA*

Received 20 September 2005; received in revised form 8 November 2005; accepted 9 November 2005

Available online 13 December 2005

Abstract

Numerical simulations are carried out for a single-channel polymer electrolyte fuel cell (PEFC) undergoing a step increase in current density. The objective is to elucidate profound interactions between the cell voltage response and water transport dynamics occurring in a low-humidity PEFC where the membrane hydration and hence resistance hinges upon the product water. Detailed results are presented to show that a step increase in the current density leads to anode dryout due to electroosmotic drag, while it takes several seconds for water back-diffusion and anode humidified gas to re-wet the anode side of the polymer membrane. The water redistribution process is controlled by water production, membrane hydration, electroosmotic drag, and water diffusion in the membrane. The anode dryout results in a substantial drop in cell voltage and hence temporary power loss. Under extreme situations such as dry anode feed, large step increase in the current density, and/or lower temperatures, the cell voltage may even reverse, resulting in not only power loss but also cell degradation. Finally, the dynamics of current distribution after a step change in gas humidification is numerically examined.

© 2005 Elsevier Ltd. All rights reserved.

Keywords: Polymer electrolyte fuel cells; Transient response; Voltage undershoot; Water transport; Load change

1. Introduction

Research on polymer electrolyte fuel cells (PEFCs) has been a rapidly growing field [1,2]. While the vast majority of efforts focus on steady-state operation of PEFCs, the dynamic behavior is of paramount importance in automotive PEFCs, given the rapid change of loads in the application.

Transient phenomena in automotive fuel cells are poorly understood at present. In addition to the complex dynamic response involving various time scales, severe degradation of MEAs in a PEFC has been observed and attributed to the transient operation; these include fuel/oxidant starvation, membrane dryout, electrode flooding, and voltage reversal [3,4]. A simple type of transients due to gas reactant transport to the catalytic sites was first explored by Um et al. [5] in 2000 and most recently further modeled by Yan et al. [6] and Shimpalee et al. [7]. This transient phenomenon typically occurs in the sub-second range.

In low-humidity PEFCs where reaction water is used to hydrate membranes, there exist profound interactions between water transport and transient cell behavior. First, there is a time scale for membrane hydration by reaction water. Furthermore, multiple mechanisms of water transport through the membrane, such as electroosmotic drag and back-diffusion, create a complex transient response involving several time scales. For example, during a step change in the current density, the electroosmotic drag will immediately remove water from the anode side of the membrane before back-diffusion of water from the cathode to anode takes effect. This can cause a temporary dryout on the anode side of the membrane and hence a jump in membrane resistance or a sharp drop in cell voltage. This voltage drop is, however, recoverable within a period of time constant characteristic of water back-diffusion through the membrane, which is dependent on the water diffusion coefficient and membrane thickness. Understanding transient behaviors of this kind is tremendously important for successful deployment of PEFC technology in vehicles.

Several papers have attempted to study transient phenomena in PEFCs experimentally. Kim et al. [8] measured the transient response of a PEFC to the load change and found a correlation between the observed overshoot or undershoot in current density

* Corresponding author. Tel.: +1 814 863 4762; fax: +1 814 863 4848.
E-mail address: cwx31@psu.edu (C.-Y. Wang).

and operating stoichiometry. Bensiger et al. [9] took a stirred tank reactor approach to examine PEFC start-up and dynamic responses to changes in load, temperature, and reactant flow rates. The importance of membrane hydration on the dynamic response of fuel cells was also pointed out based on their experimental data. Tsushima et al. [10] measured the spatial profile of water content in a thick polymer membrane in an operating PEFC using magnetic resonance imaging (MRI), and indicated that water content on the anode side of the membrane decreased significantly within 200 s of cell start-up, causing a rapid drop in cell voltage. The use of very thick membranes in their work was required by coarse spatial resolution of MRI, i.e. $>25 \mu\text{m}$.

Detailed modeling of the intricate interactions between transient water transport characteristics and voltage response has been absent in the literature. Previous modeling studies were mostly based on simplified models and did not address the controlling transient phenomena in low-humidity PEFCs for modern applications. The model of Amphlett et al. [11,12] was based on coupling the steady-state electrochemical kinetic equation with an unsteady, lumped-parameter thermal model. The one-dimensional model developed by Ceraolo et al. [13] considered the cathode side and ignored the important coupling of water transport through the polymer membrane and electrochemical water production. Xie et al. [14] and Pathapati et al. [15] developed a system-level dynamic model using lumped-parameters in each sub-system. The transient water transport model of Okada et al. [16] was restricted to the membrane region, and the coupling between membrane water uptake/transport and electrochemical production of water has been simplified by setting boundary conditions to the two sides of the membrane. Further, since only the water transport equation was solved, prediction of dynamic responses of cell currents and voltages was beyond their model capability. Their model was later adopted to study the transient behavior of water and influence of the impurity ions [17].

Most recently, a three-dimensional transient model, coupling the species transport, gas flow, and water transport through the membrane with electrochemical kinetics in catalyst layers, was developed by Wang and Wang [18]. The transient model considers vastly different time scales characteristic of the electrochemical double layer discharging, gas transport, and membrane hydration, respectively. In addition, numerical exploration of the transients after a step change in cell voltage or inlet humidity was carried out. However, to date no study has been carried out on the transient response of a low-humidity PEFC to step changes in current load, which is the standard operational mode of load changes in the automotive application.

In the present work, the previous model presented in Ref. [18] is further extended by solving, in addition, the electron transport equation [19], making it possible to study the transient response of a PEFC to a step change in current density. Dynamic responses of a single-channel PEFC with Gore[®] 18 μm and Nafion[®] 112 membranes are numerically explored under both fully humidified and relatively dry cathode conditions.

2. Mathematical model

2.1. Governing equations

The model equations include the following laws of conservation [18,19]:

$$\text{Continuity : } \nabla \cdot \vec{u} = 0 \quad (1)$$

$$\begin{aligned} \text{Momentum : } & \frac{1}{\varepsilon} \left[\frac{\partial \vec{u}}{\partial t} + \frac{1}{\varepsilon} \nabla \cdot (\vec{u}\vec{u}) \right] \\ & = -\nabla \left(\frac{p}{\rho} \right) + \nabla \cdot \tau + S_u \end{aligned} \quad (2)$$

$$\text{Species : } \varepsilon \frac{\partial C_k}{\partial t} + \nabla \cdot (\vec{u}C_k) = \nabla \cdot (D_k^{\text{eff}} \nabla C_k) + S_k \quad (3)$$

$$\text{Proton charge : } 0 = \nabla \cdot (\kappa^{\text{eff}} \nabla \Phi_e) + S_{\Phi_e} \quad (4)$$

$$\text{Electron charge : } 0 = \nabla \cdot (\sigma^{\text{eff}} \nabla \Phi_s) + S_{\Phi_s} \quad (5)$$

where porosity ε becomes unity in gas channels. A constant gas density is assumed in Eqs. (1) and (2). Moreover, Eq. (3) encompasses the water transport equation in the MEA, where the effective factor in the transient term, ε , is expressed as:

$$\varepsilon = \varepsilon_g + \varepsilon_m \frac{dC_w^m}{dC_w} = \varepsilon_g + \varepsilon_m \frac{\rho_m RT}{EW} \frac{d\lambda}{p^{\text{sat}} da} \quad (6)$$

where ρ_m is the density of a dry membrane and the membrane water content, λ , can be calculated from [20]:

$$\lambda = \begin{cases} 0.043 + 17.81a - 39.85a^2 + 36.0a^3, & 0 < a \leq 1 \\ 14 + 1.4(a - 1), & 1 \leq a \leq 3 \\ 16.8, & 3 < a \end{cases} \quad (7)$$

The water activity, a , is defined as:

$$a = \frac{C_w RT}{p^{\text{sat}}} \quad (8)$$

where the water vapor partial pressure is calculated by:

$$\begin{aligned} \log_{10} p^{\text{sat}} &= -2.1794 + 0.02953(T - 273.15) - 9.1837 \\ &\quad \times 10^{-5}(T - 273.15)^2 + 1.4454 \\ &\quad \times 10^{-7}(T - 273.15)^3 \end{aligned} \quad (9)$$

The various source terms, S , electrochemical and physical properties are listed in Tables 1–3, respectively. In addition, the present model is based on molar concentration and assumes constant gas density and no mass source in the continuity and momentum equations. The validity of these assumptions was justified in Ref. [21]. In addition, a complete form of the electron transport equation should include a transient term representing the electrochemical double layer discharging [22]. However, as discussed in Ref. [18], the time constant of the double layer discharging ranges from micro- to milli-seconds, sufficiently short to be safely neglected for automotive fuel cells.

Table 1
Source terms for the conservation equations in each region [18,19]

	S_u	S_k	S_{ϕ_e}	S_{ϕ_s}
Gas channels	0	0	–	–
Diffusion layers	$-\frac{\mu}{K_{GDL}} \vec{u}$	0	0	0
Catalyst layers	$-\frac{\mu}{K_{CL}} \vec{u}$	$-\nabla \cdot \left(\frac{n_d}{F} i_e \right) - \frac{s_k j}{nF}$	j	$-j$
Membrane	–	0	0	0

Electrochemical reaction: $\sum_k s_k M_k^z = ne^-$

where

$\left\{ \begin{array}{l} M_k^z \text{ is the chemical formula of} \\ \text{species, } s_k \text{ the stoichiometry coef-} \\ \text{ficient and } n \text{ is the number of elec-} \\ \text{trons transferred} \end{array} \right.$

In PEM fuel cells, there are:

(Anode) $H_2 - 2H^+ = 2e^-$

(Cathode) $2H_2O - O_2 - 4H^+ = 4e^-$

Note: n_d is the electroosmotic drag coefficient for water. For H_2 and O_2 , $n_d = 0$.

Table 2
Electrochemical properties

Description	Anode	Cathode
Transfer current density, j (A/m ³)	$ai_{0,a} \left(\frac{C_{H_2}}{C_{H_2,ref}} \right)^{1/2} \left(\frac{\alpha_a + \alpha_c}{RT} \cdot F \cdot \eta \right)$	$-ai_{0,c} \left(\frac{C_{O_2}}{C_{O_2,ref}} \right) e^{-(\alpha_c F/RT) \cdot \eta}$
Surface overpotential, η (V)	$\Phi_s - \Phi_e - U_0$	$\Phi_s - \Phi_e - U_0$
Equilibrium potential, U_0 (V)	0	$1.23 - 0.9 \times 10^{-3}(T - 298)$
Exchange current density \times reaction surface area, ai_0 (A/m ³)	1.0×10^9	10000
Transfer coefficient, α	$\alpha_a + \alpha_c = 2$	$\alpha_c = 1$

2.2. Boundary and initial conditions

Eqs. (1)–(5) form a complete set of governing equations with nine unknowns: \vec{u} (three components), P , C_{H_2} , C_{O_2} , C_{H_2O} , ϕ_e , and ϕ_s . Their corresponding boundary and initial conditions are described as follows.

2.2.1. Flow inlet boundaries

The inlet velocity \vec{u}_{in} in a gas channel is expressed by the respective stoichiometric flow ratio, i.e. ξ_a or ξ_c , defined at a reference current density, I_{ref} , as:

$$\xi_a = \frac{C_{H_2} \rho_a u_{in,a} A_a}{\frac{I_{ref} A}{2F}} \quad \text{and} \quad \xi_c = \frac{C_{O_2} \rho_c u_{in,c} A_c}{\frac{I_{ref} A}{4F}} \quad (10)$$

where A_a and A_c are the flow cross-sectional areas of the anode and cathode gas channels, respectively. The inlet molar concentrations are determined by the inlet pressure and humidity according to the ideal gas law.

2.2.2. Outlet boundaries

Fully developed or no-flux conditions are applied:

$$\frac{\partial \vec{u}}{\partial n} = 0, \quad \frac{\partial C_k}{\partial n} = 0, \quad \frac{\partial \phi_e}{\partial n} = 0, \quad \frac{\partial \phi_s}{\partial n} = 0 \quad (11)$$

2.2.3. Walls

No-slip and impermeable velocity condition and no-flux condition are applied:

$$\vec{u} = 0, \quad \frac{\partial C_k}{\partial n} = 0, \quad \frac{\partial P}{\partial n} = 0, \quad \frac{\partial \phi_e}{\partial n} = 0 \quad (12)$$

Table 3
Physical and transport properties

Quantity	Value	Reference
Ionic conductivity of membrane, κ	$(0.005139\lambda - 0.00326) \exp \left[1268 \left(\frac{1}{303} - \frac{1}{T} \right) \right]$	Springer et al. [20]
H_2O diffusivity in membrane, D_w^m	$D_w^m = \begin{cases} 3.1 \times 10^{-3} \lambda (e^{0.28\lambda} - 1) \cdot e^{-2346/T}, & \text{for } 0 < \lambda \leq 3 \\ 4.17 \times 10^{-4} \lambda (1 + 161 e^{-\lambda}) \cdot e^{-2346/T}, & \text{otherwise} \end{cases}$	Motupally et al. [25]
Electroosmotic drag coefficient, n_d	$n_d = \begin{cases} 1.0, & \text{for } \lambda \leq 14 \\ \frac{1.5}{8} (\lambda - 14) + 1.0, & \text{otherwise} \end{cases}$	Zawodzinski et al. [26]
Dry membrane density, ρ_m	1.98×10^3	West and Fuller [27]
H_2/O_2 diffusivity in membrane, $D_{H_2}^m/D_{O_2}^m$	$2.59 \times 10^{-6}/1.22 \times 10^{-6}$	Bernardi and Verbrugge [28]
Gas diffusion coefficient in porous media, D^{eff}	$D^{eff} = \frac{\epsilon}{\tau} D_0 \left(\frac{T}{333} \right)^{3/2} \left(\frac{1}{p} \right)$	Bird et al. [29]
Viscosity of anode/cathode gas, μ	$\mu = 9.88 \times 10^{-6} X_{H_2} + 1.12 \times 10^{-5} X_{H_2O} + 2.01 \times 10^{-5} X_{N_2} + 2.3 \times 10^{-5} X_{O_2}$	Incropera and DeWitt [30]

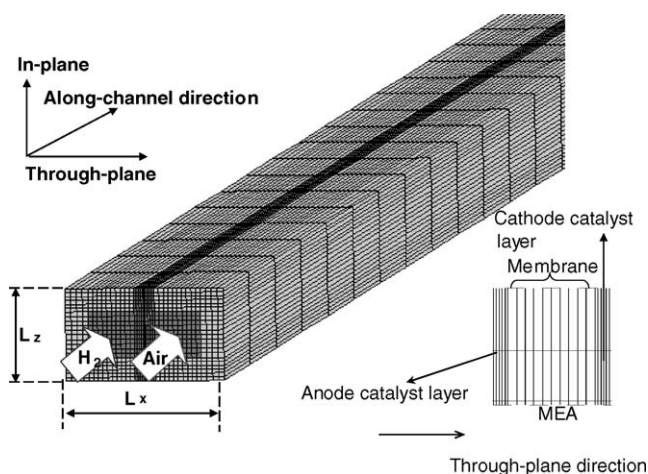


Fig. 1. Computational domain and mesh of a single-channel PEFC.

In addition, the boundary conditions for the electronic phase potential, ϕ_s , at the bipolar plate outer surfaces can be expressed as [23]:

$$\begin{cases} \frac{\partial \phi_s}{\partial n} = I, & \text{anode} \\ \frac{\partial \phi_s}{\partial n} = -I, & \text{cathode} \\ \frac{\partial \phi_s}{\partial n} = 0, & \text{otherwise} \end{cases} \quad (13)$$

2.2.4. Initial conditions

The initial conditions are either zero or a steady-state field from a previous operating point.

2.3. Numerical procedures

The conservation equations are solved using a commercial computational fluid dynamics (CFD) package, Star-CD[®], with PISO algorithm, the pressure implicit splitting of operators [24]. PISO is based on predictor–corrector splitting for unsteady problems. The specific governing equations with appropriate source terms developed herein are incorporated in a user code. An average current density is specified as an input parameter, allowing the local current density and electronic phase potential to vary spatially according to local conditions. Thus, the load change is performed through manipulation of the cell current, i.e. electron flux, on the bipolar plate surfaces. The mesh of a single-channel PEFC is shown in Fig. 1. Table 4 lists the geometry and physical parameters. To accurately describe the electrochemical, hydration, and transport processes in the MEA, 10 grids are employed within the membrane and 6 grids are placed in the catalyst layer in the through-plane direction. Approximately 100,000 computational gridpoints are used to capture the detailed three-dimensional electrochemical and transport phenomena. Adaptive time stepping is used in which the current time step is made inversely proportional to the temporal gradient of current density at the previous time step with the maximum of 0.1 s.

Table 4
Geometrical and physical parameters [21,31]

Quantity	Value
Gas channel depth/width (mm)	1.0/1.0
Shoulder width (mm)	1.0
GDL/catalyst layer thickness, δ_{GDL}/δ_{CL} (mm)	0.3/0.01
Membrane thickness (Gore [®] 18 μm /Nafion [®] 112), δ_m (mm)	0.018/0.051
Cell thickness/length (mm)	2.0/100.0
Anode/cathode pressures, P (atm)	2.0/2.0
Stoichiometric flow ratio ξ in anode/cathode	1.5/2.0
Cell temperature (K)	353.15
Porosity of diffusion layer/catalyst layer, $\varepsilon/\varepsilon_g$	0.6/0.4
Volume fraction of ionomer in catalyst layer, ε_m	0.26
Permeability of GDL/catalyst layer, K_{GDL}/K_{CL} (m^2)	$10^{-12}/10^{-15}$
$\text{H}_2/\text{H}_2\text{O}$ diffusivity in anode gas at standard condition, $D_{\text{O}_2,\text{H}_2,\text{a}}/D_{\text{O}_2,\text{w},\text{a}}$ (m^2/s)	$1.1 \times 10^{-4}/1.1 \times 10^{-4}$
$\text{O}_2/\text{H}_2\text{O}$ diffusivity in cathode gas at standard condition, $D_{\text{O}_2,\text{O}_2,\text{c}}/D_{\text{O}_2,\text{w},\text{c}}$ (m^2/s)	$3.24 \times 10^{-5}/3.89 \times 10^{-5}$

3. Results and discussion

A single-channel PEFC with Gore[®] 18 μm and Nafion[®] 112 (i.e. 51 μm) membranes, respectively, is chosen for a parametric study. While the focus of the present work is on elucidating dynamic behaviors under low-humidity operation, a fully humidified case is also simulated for comparison in which there exist the transients of gas transport only and the transient membrane hydration becomes irrelevant as the membrane remains always hydrated. All results are intended to explore the transient response to a step change from one steady state to another. The two types of step changes under consideration are in the current density and cathode inlet relative humidity.

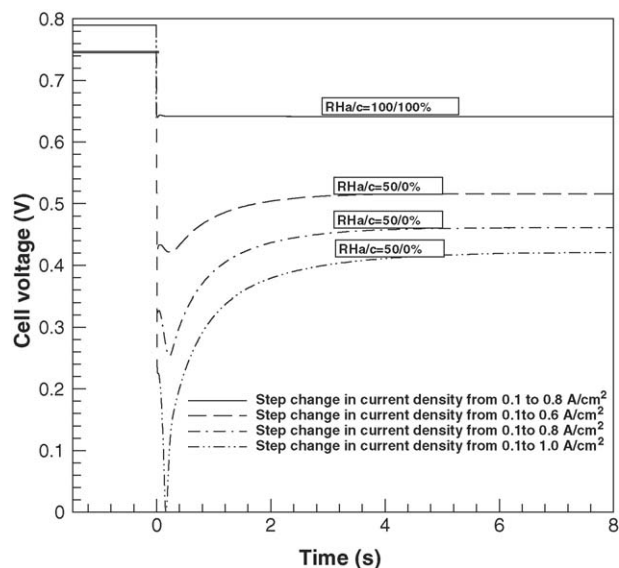


Fig. 2. Dynamic response of cell voltage to the step change in current density in a PEFC using Gore[®] 18 μm membrane.

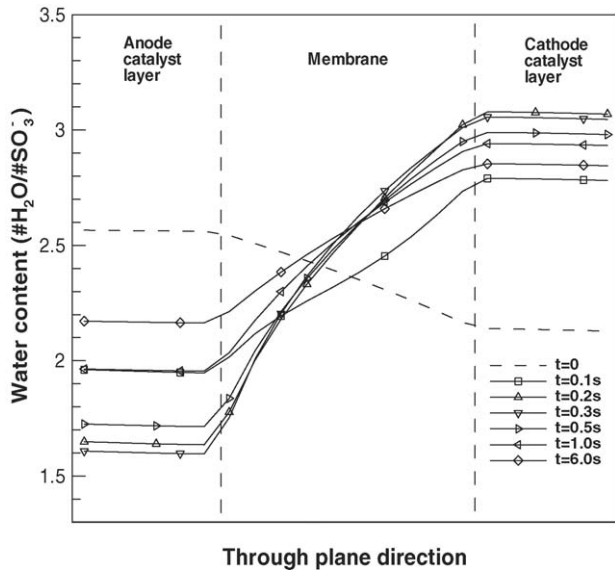


Fig. 3. Dynamic profiles of water content in the MEA after the step change in current density from 0.1 to 0.8 A/cm² under dry operation (RH_{a/c} = 50/0%) at the 10% fractional distance of the PEFC with Gore[®] 18 μm membrane.

Fig. 2 shows the dynamic response of cell voltage to a current step increase under various operating conditions. It can be seen that the voltage response is nearly instantaneous under the fully humidified condition, while it takes several seconds for low-humidity cells to attain another steady state. In addition, the dynamic behavior of all low-humidity cases exhibits a voltage undershoot. The degree of undershoot increases with the magnitude of current change. When the current density is changing from 0.1 to 1.0 A/cm², the cell voltage drops to zero. With a larger current increase (i.e. >1.0 A/cm²), the PEFC will reverse the voltage and may lead to cell degradation.

To further explore explanations for the voltage undershoot, Figs. 3–5 present the water content profiles in the MEA at vari-

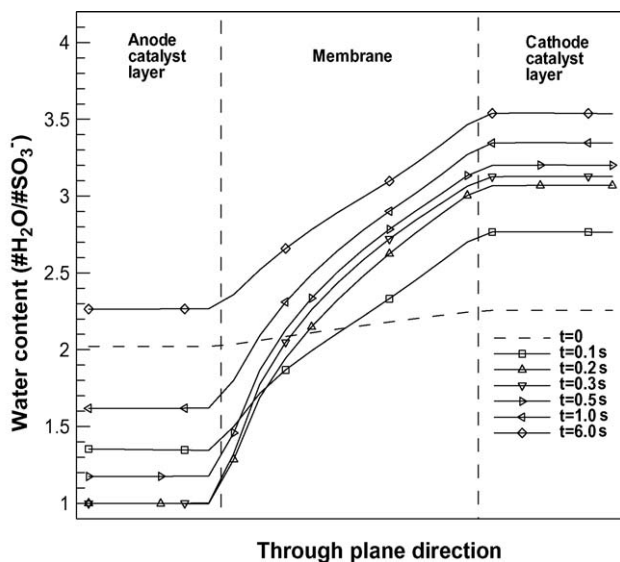


Fig. 4. Dynamic profiles of water content in the MEA after the step change in current density from 0.1 to 0.8 A/cm² under dry operation (RH_{a/c} = 50/0%) at the 50% fractional distance of the PEFC with Gore[®] 18 μm membrane.

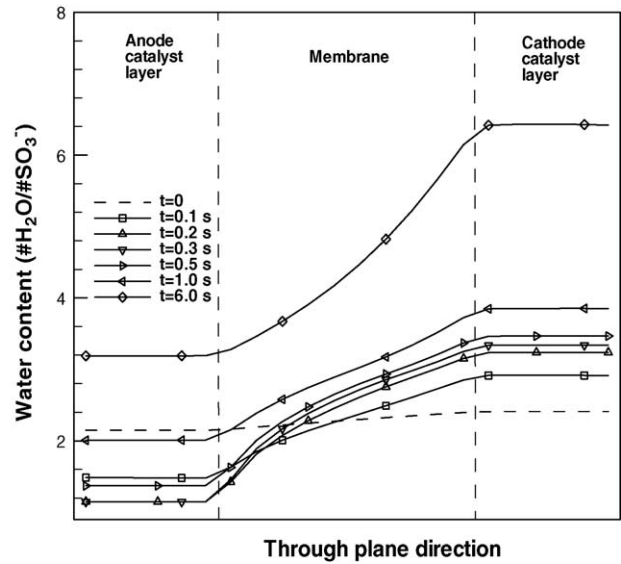


Fig. 5. Dynamic profiles of water content in the MEA after the step change in current density from 0.1 to 0.8 A/cm² under dry operation (RH_{a/c} = 50/0%) at the 90% fractional distance of the PEFC with Gore[®] 18 μm membrane.

ous time instants and at three locations in the PEFC, respectively, after the current density changes from 0.1 to 0.8 A/cm². In these figures, dashed lines denote the initial water content profiles immediately before the current change, and solid lines at $t = 6$ s mark the final profiles at the new steady state. It can be seen from Figs. 3–5 that just after the step change, the water content in the anode decreases while that in the cathode increases. This can be explained by the water electroosmotic drag, which increases directly proportionally to the current density jump. The anode hydration levels reach lowest around 0.3 s after the step change, roughly the same time as the cell voltage reaching the minimum as shown in Fig. 2. After that time instant, the anode begins to get water through back-diffusion as the difference of water concentration between the anode and cathode is enlarged. The water profiles reach steady state around 6 s, which is of the same order as the time constant of membrane hydration [18], i.e. $\tau_{m,H} = \frac{\rho_m \Delta \lambda}{EW} \sim 7$ s. In addition, the time constant of

water diffusion across the membrane, i.e. $\tau_{m,D} = \frac{\delta_m^2}{D_m^{eff}} \sim 0.2$ s at $\lambda = 3$, coincides with the time when the cell voltage reaches the minimum, indicating that back-diffusion begins to rehydrate the anode. A difference between these three figures at different fractional distances into the PEFC is that the water content goes up higher in the downstream of the cell, due to the effect of water production.

Fig. 6 displays variations of the water molar concentration profile in the anode channel with time after the step change. Once again, the dashed line represents the initial condition before the step change, and the solid line at $t = 6$ s is the new steady state. It is interesting to note that the water concentration in the anode channel strongly responds to the step change in current density. Further, there is significant dryout of the anode stream in the downstream region during transients. This phenomenon can be explained by the fact that most of water carried

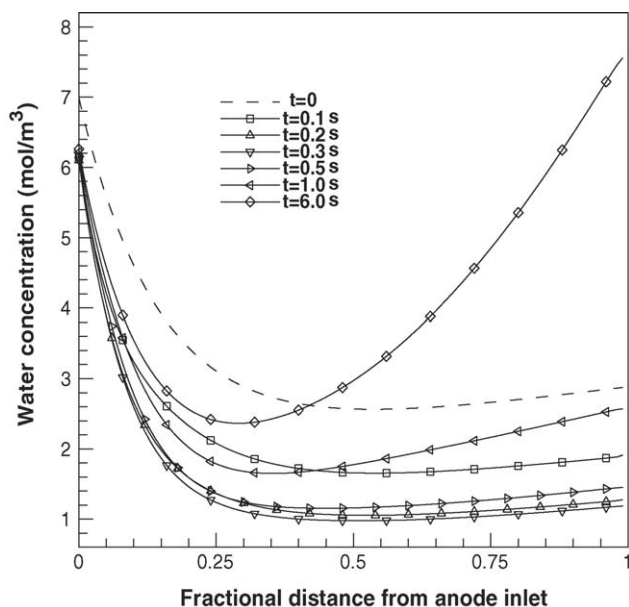


Fig. 6. Water concentration profiles in the anode gas channel after the step change in current density from 0.1 to 0.8 A/cm² under dry operation ($RH_{a/c} = 50/0\%$) and with Gore[®] 18 μm membrane.

in partially humidified anode inlet gas is transferred to the cathode in the upstream region due to the fast gas transport across the anode GDL with a time constant around 0.01–0.1 s [18], leaving the downstream region temporarily dry. Once the water back-diffusion through the membrane takes effect, the water concentration in the anode downstream recovers. In addition, note that the present model assumes a constant gas density and no mass source. Thus, the anode flow remains constant along the channel and the change in the water profile shown in this figure is not due to the flow variation with time.

As a result of water redistribution during transients, the membrane resistance experiences an overshoot, as shown in Fig. 7. As indicated by the dashed line, the spatially resolved membrane resistance in this low-humidity cell at the initial state is seen to increase first along the flow direction, due to the anode dehydration under the influence of electroosmotic drag, and then decrease due to water production within the cell. The same spatial trend remains at the final steady state with much higher current density, except that the anode dehydration region is shortened due to the much higher production rate of water on the cathode; see the solid line at $t = 6$ s. In transition, the membrane resistance initially increases overall before drop-down, indicating the significant role played by dehydration of the anode side of the membrane. In addition, significant decrease in the membrane resistance occurs in the downstream due to higher water production on the cathode, in accordance with that shown in Fig. 4.

Fig. 8 shows that the ionic resistance in the cathode, despite an eight-fold increase in water production, does not decrease uniformly: the substantial decrease in the ionic resistance in the cathode catalyst layer begins only after $\sim 30\%$ fractional distance into the fuel cell. An interesting phenomenon occurs in the anode catalyst layer, as shown in Fig. 9: the anode ionic resis-

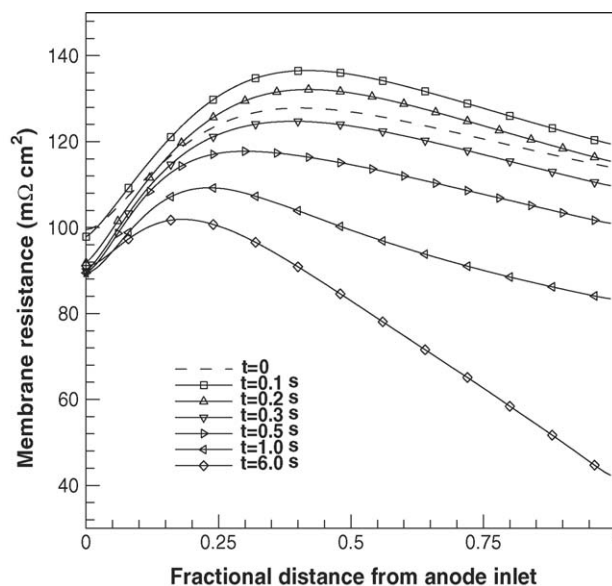


Fig. 7. Dynamic profiles of the membrane resistance after the step change in current density from 0.1 to 0.8 A/cm² under dry operation ($RH_{a/c} = 50/0\%$) and with Gore[®] 18 μm membrane.

tance shows a substantial increase within initial 0.2 s followed by a reduction over the next 1 s. The resistance increment during transients is several fold, although the anode hydration level only shows a small decrease as indicated in Figs. 2–4. The reason can be explained by the non-linear relation between water content and ionic conductivity as shown in Table 3, which indicates that the proton conductivity or inversely the ionic resistance is quite sensitive to water content at low hydration levels. In addition, it is noted that the anode ionic resistance during transients is much higher than those in the membrane and cathode catalyst layer, indicating its controlling role in fuel cell dynamics.

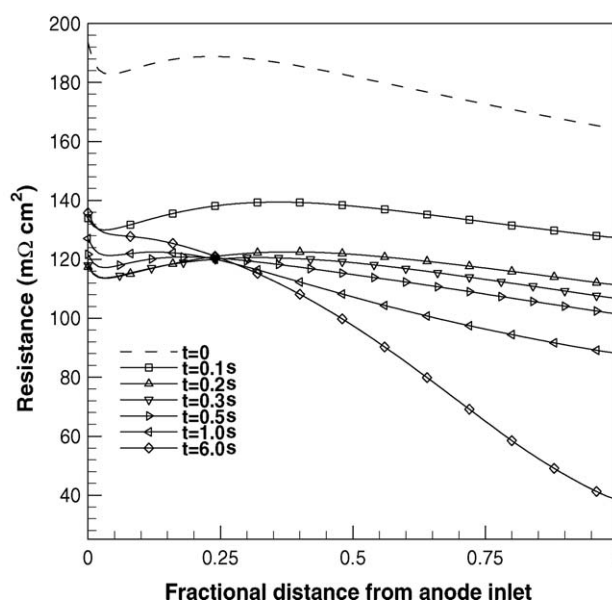


Fig. 8. Dynamic profiles of the ionic resistance in the cathode after the step change in current density from 0.1 to 0.8/cm² under dry operation ($RH_{a/c} = 50/0\%$) and with Gore[®] 18 μm membrane.

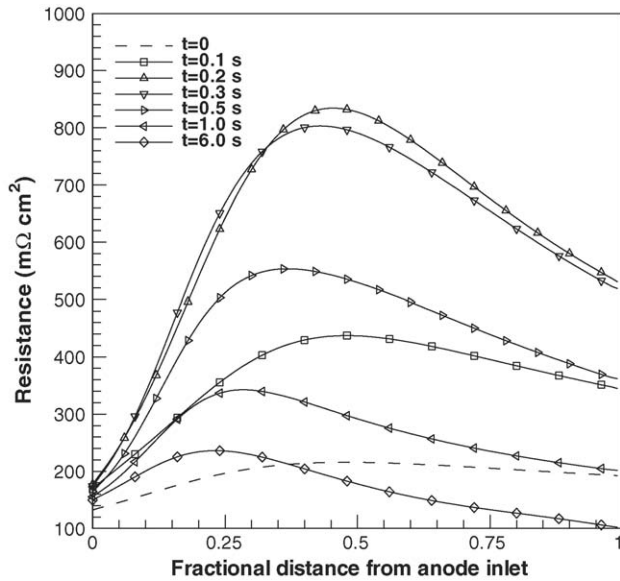


Fig. 9. Dynamic profiles of the ionic resistance in the anode after the step change in current density from 0.1 to 0.8 A/cm² under dry operation ($RH_{a/c} = 50/0\%$) and with Gore[®] 18 μm membrane.

Fig. 10 presents the history of the local current density profile after the step change. A drastic redistribution of the local current density occurs during fast transients of about 1 s, while the average at any time instant remaining the same as the imposed cell current density. Upon the constant average current density imposed, the protons would prefer to flow in the low resistance region, namely the low anode ionic resistance region, which occurs near the flow inlet during the initial period. Consequently, high current density first appears in the upstream region and then shifts to the downstream as the anode ionic resistance is lowered there. The profiles of local current density shown in Fig. 10 also

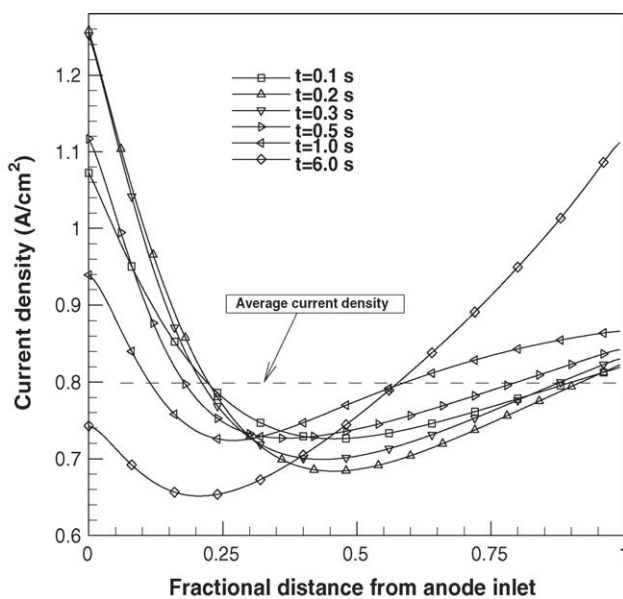


Fig. 10. Dynamic profiles of the local current density after the step change in average current density from 0.1 to 0.8 A/cm² under dry operation ($RH_{a/c} = 50/0\%$) and with Gore[®] 18 μm membrane.

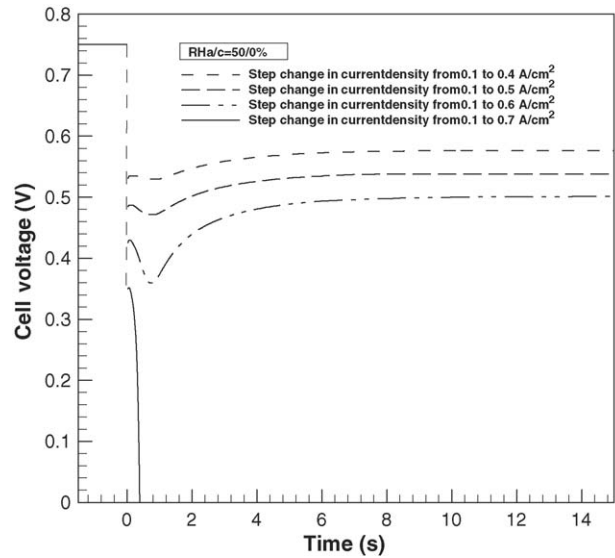


Fig. 11. Dynamic response of cell voltage to the step change in current density in a PEFC using Nafion[®] 112 membrane.

help explain the dynamic changes seen in Fig. 8 for the cathode catalyst layer resistance. Because much higher current density occurs initially at the inlet, water production there dramatically decreases the ionic resistance in the cathode, while the resistance bounces back when the local current density in the upstream decreases again.

From the above analysis of the dry cell using Gore[®] 18 μm membrane, it can be seen that dynamic balance between water back-diffusion and electroosmotic drag causes temporary dryness in the anode and hence dictates the cell performance response. To further elucidate this dynamic water balance in the membrane, a comparative case is simulated for a thicker membrane, i.e. Nafion[®] 112. The corresponding time responses of cell voltage are shown in Fig. 11 under the same humidification conditions, i.e. $RH_{a/c} = 50/0\%$. It can be seen that the voltage undershoot is much more severe for the thicker membrane as compared with Fig. 2, and the current density increase cannot even go beyond 0.7 from 0.1 A/cm², without causing zero voltage. In addition, the time period in which back-diffusion of water begins to take effect triples that of the Gore[®] 18 μm membrane. A similar calculation of $\tau_{m,D} = \frac{\delta_m^2}{D_m^{eff}}$ for the membrane thickness of 51 μm yields ~ 0.8 s for the time constant of water diffusion across the membrane (at $\lambda = 3$).

Fig. 12 shows dynamic profiles of water content in the MEA after the step change under dry operation ($RH_{a/c} = 50/0\%$) at the mid-length of the PEFC using Nafion[®] 112 membrane. It is seen that the thicker membrane delays rehydration of the anode by water back-diffusion, thus amplifying the effect of electroosmotic drag on anode water loss. In addition, this figure, along with Figs. 3–5, underscores the importance of the non-linear description of water transport in the membrane during transients. A lumped parameter model or simplified analytical model would fail to capture this feature.

Fig. 13 shows the response of cell voltage to a reverse step change, i.e. step decrease in current density from 0.8 to

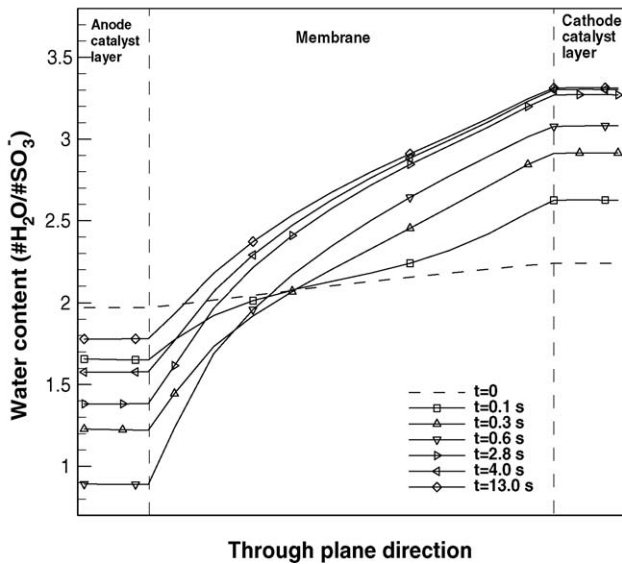


Fig. 12. Dynamic profiles of water content in the MEA after the step change in current density from 0.1 to 0.6 A/cm² under dry operation (RH_{a/c} = 50/0%) at the 50% fractional distance of the PEFC with Nafion[®] 112 membrane.

0.1 A/cm², under a dry and a wet case, respectively. While the initial and final steady states reverse their voltage values, the transient behavior is generally gradual and smooth in both dry and wet cases. In practice, vehicle deceleration could be more problem-free under dry operating conditions as there will be no concern for electrode and channel flooding. In contrast, a current density step decrease and ensuing reduction in gas flow rates under the fully humidified conditions may trigger severe flooding in electrodes and channels, a topic that is beyond the scope of the present work.

Fig. 14 presents the time responses of cell voltage to the changes in the humidification conditions, using Gore[®] 18 μm membrane. At a constant current density, the change in cell

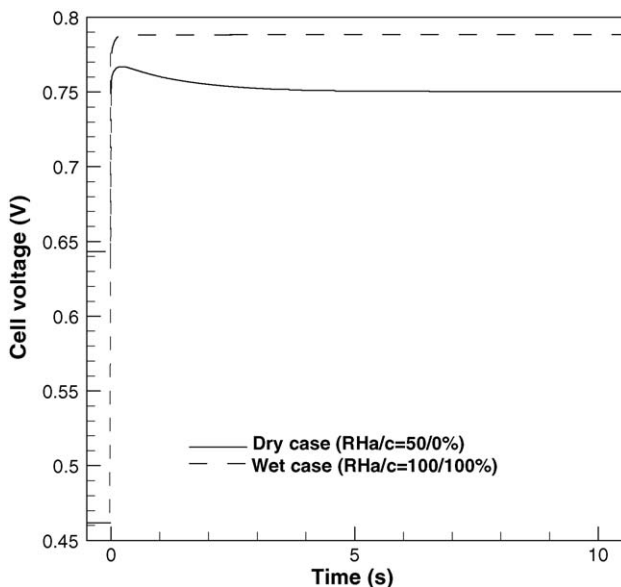


Fig. 13. Dynamic response of cell voltage to the step change in current density from 0.8 to 0.1 A/cm² in a PEFC using Gore[®] 18 μm membrane.

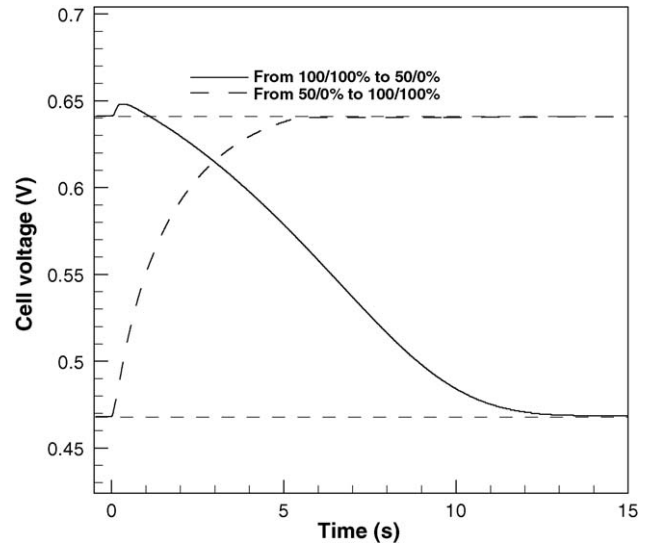


Fig. 14. Dynamic responses of cell voltages after the step changes in the humidification conditions at the current density of 0.8 A/cm² in a PEFC using Gore[®] 18 μm membrane.

voltage is mainly attributed to the ohmic loss or membrane resistance variation corresponding to a varying hydration level. In the case of RH_{a/c} = 50/0% switched to 100/100%, the cell voltage keeps increasing, indicating that the membrane becomes better hydrated by the humidity introduced in the cell. A similar conclusion can be drawn for the reverse case, except for a slight voltage overshoot in the initial split second. Occurrence of this overshoot can be explained by the richer oxygen contained in the less-humidified inlet cathode air.

It is of great interest to study the redistribution of current density after a step change in external humidification. Fig. 15 depicts the time variations in the local current density profile when the external gas humidification switches from RH_{a/c} = 100/100 to

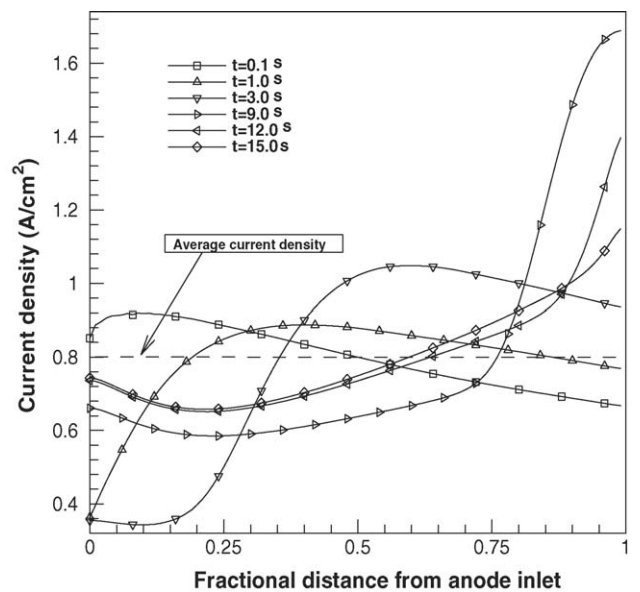


Fig. 15. Dynamic profiles of the local current density after the step changes in humidification conditions from RH_{a/c} = 100/100 to 50/0% under the current density of 0.8 A/cm² in a PEFC, using Gore[®] 18 μm membrane.

50/0% under the average current density of 0.8 A/cm^2 . It can be seen that initially the local current density is higher upstream and lower downstream, a pattern primarily controlled by oxygen depletion and characteristic of fully humidified cells. With time, however, the current density in the upstream region drops due to drier gas supply there, which leaves more oxygen molecules downstream to produce high current density (also benefited from more humidified gases and hence hydrated membrane by product water). Eventually, the current density profile at the new steady state attains an increasing pattern indicative of the membrane hydration control commonly occurring in low-humidity cells. Note that the local current density can temporarily reach 1.6 A/cm^2 during transients, a level substantially beyond steady-state values. This overshoot in local current density may have important implications for PEFC durability where membrane and catalyst degradation is strongly tied to the current density. A more detailed discussion on membrane hydration/dehydration can be found in Ref. [18].

4. Conclusions

Numerical simulations of a single-channel PEFC with Gore[®] $18 \mu\text{m}$ and Nafion[®] 112 membranes have been carried out to study the intricate transient phenomena under current density step changes, with focus primarily on dry cell operation. Detailed numerical results are presented to illustrate the dynamics of water transport through the membrane. Specifically, it is found that a step increase in the current density instantaneously dries out the anode under the influence of electroosmotic drag, while it takes several seconds, consistent with theoretical estimation, for the water back-diffusion to rehydrate the anode. The water redistribution process in the PEFC, directly impacting the cell voltage response, is controlled by dynamic balance between electroosmotic drag and back-diffusion in the membrane characterized by two disparate time scales. In addition, the present numerical study reveals that the change in gas humidification conditions will lead to a drastic fluctuation of the local current density during transients. This finding may lend new insight into PEFC degradation caused from fast-transient cycling.

Future work could include a parametric study of membrane properties, particularly the water diffusivity and electroosmotic drag coefficient in the membrane, water uptake, and ionomer equivalent weight. In addition, the impact of alternative membranes (e.g. hydrocarbon membranes) on the PEFC transients is worthy of assessment using the present model.

Acknowledgement

Support for this work is provided, in part, by Ford Motor Company.

Appendix A. Nomenclature

a water activity or effective catalyst area per unit volume (m^2/m^3)

A	superficial electrode area (m^2)
C_{dl}	capacitance of the double layer (mF/cm^2)
C_k	molar concentration of species k (mol/m^3)
D	mass diffusivity of species (m^2/s)
EW	equivalent weight of dry membrane (kg/mol)
F	Faraday's constant, $96,487 \text{ C/equivalent}$
i_0	exchange current density (A/m^2)
i_e	superficial current density (A/m^2)
I	current density (A/cm^2)
j	transfer current (A/cm^3)
K	permeability (m^2)
n	the direction normal to a surface
n_d	electroosmotic drag coefficient, $\text{H}_2\text{O}/\text{H}^+$
P	pressure (Pa)
R	gas constant, $8.134 \text{ J}/(\text{mol K})$
RH	relative humidification
s	stoichiometry coefficient in electrochemical reaction
$yu S$	source term in transport equations
t	time (s)
T	temperature (K)
\vec{u}	velocity vector (m/s)
V_{cell}	cell potential (V)
X	mole fraction

Greek letters

α	transfer coefficient
δ	thickness (m)
ε	porosity
η	surface overpotential (V)
κ	ionic conductivity (S/m)
λ	membrane water content
μ	viscosity ($\text{kg}/(\text{m s})$)
ξ	stoichiometric flow ratio
ρ	density (kg/m^3)
σ	electronic conductivity (S/cm)
τ	shear stress (N/m^2); time constant (s); tortuosity factor
ϕ	phase potential (V)

Superscripts and subscripts

a	anode
c	cathode
ch	channel
CL	catalyst layer
dl	double layer
e	electrolyte
eff	effective value
g	gas phase
GDL	gas diffusion layer
in	inlet
k	species
m	membrane phase; membrane
o	standard condition, 273.15 K and 101.3 kPa (1 atm)
ref	reference
s	electronic phase
sat	saturate value
w	water

References

- [1] C.-Y. Wang, *Chem. Rev.* 104 (2004) 4727.
- [2] M.L. Perry, T.F. Fuller, *J. Electrochem. Soc.* 149 (7) (2002) 59.
- [3] D.P. Wilkison, J. St.-Pierre, in: W. Vielstich, H. Gasteiger, A. Lamm (Eds.), *Handbook of Fuel Cells: Fundamentals, Technology and Applications*, vol. 3, John Wiley & Sons Ltd., 2003.
- [4] S.D. Knight, K.D. Colbow, J. St.-Pierre, D.P. Wilkinson, *J. Power Sources* 127 (2004) 127.
- [5] S. Um, C.-Y. Wang, K.S. Chen, *J. Electrochem. Soc.* 147 (2000) 4485.
- [6] W. Yan, C.-Y. Soong, F. Chen, H.-S. Chu, *J. Power Sources* 143 (2005) 48.
- [7] S. Shimpalee, W.-K. Lee, J.W. Van Zee, H. Naseri-Neshat, *J. Power Sources*, in press.
- [8] S. Kim, S. Shimpalee, J.W. Van Zee, *J. Power Sources* 135 (2004) 110.
- [9] J. Bensiger, E. Karnas, J. Moxley, C. Teuscher, I.G. Kevrekidis, *AIChE J.* 50 (2004) 1889.
- [10] S. Tsushima, K. Teranishi, S. Hirai, *J. Electrochem. Soc.* 7 (9) (2004) 269.
- [11] J.C. Amphlett, R.F. Mann, B.A. Peppley, P.R. Roberge, A. Rodrigues, *J. Power Sources* 61 (1996) 183.
- [12] J.C. Amphlett, E.H. de Olivera, R.F. Mann, P.R. Roberge, A. Rodrigues, J.P. Salvador, *J. Power Sources* 65 (1997) 173.
- [13] M. Ceraolo, C. Miulli, A. Pozio, *J. Power Sources* 113 (2003) 131.
- [14] X. Xie, J. Tang, A. Smirnova, R. England, N. Sammes, J. Power Sources 133 (2004) 188.
- [15] P.R. Pathapati, X. Xue, J. Tang, *Renewable Energy* 30 (2005) 1.
- [16] T. Okada, G. Xie, Y. Tanabe, *J. Electroanal. Chem.* 413 (1996) 49.
- [17] F. Chen, Y. Su, C. Soong, W. Yan, H. Chu, *J. Electroanal. Chem.* 566 (2004) 85.
- [18] Y. Wang, C.-Y. Wang, *Electrochim. Acta* 50 (2005) 1307.
- [19] H. Meng, C.-Y. Wang, *J. Electrochem. Soc.* 151 (2004) 358.
- [20] T.E. Springer, T.A. Zawodinski, S. Gottesfeld, *J. Electrochem. Soc.* 126 (1991) 2334.
- [21] Y. Wang, C.-Y. Wang, *J. Electrochem. Soc.* 152 (2) (2005) 445.
- [22] I.J. Ong, J. Newman, *J. Electrochem. Soc.* 146 (12) (1999) 4360.
- [23] H. Meng, C.-Y. Wang, *Fuel Cells*, in press.
- [24] R.I. Issa, *J. Comp. Phys.* 62 (1986) 40.
- [25] S. Motupally, A.J. Becker, J.W. Weidner, *J. Electrochem. Soc.* 147 (2000) 3171.
- [26] T.A. Zawodzinski, J. Davey, J. Valerio, S. Gottesfeld, *Electrochim. Acta* 40 (1995) 297.
- [27] A.C. West, T.F. Fuller, *J. Appl. Electrochem.* 26 (1996) 557.
- [28] D.M. Bernardi, M.W. Verbrugge, *J. Electrochem. Soc.* 139 (1992) 2477.
- [29] R.B. Bird, W.E. Stewart, E.N. Lightfoot, *Transport Phenomena*, John Wiley & Sons, New York, 1960.
- [30] F.P. Incropera, D.P. DeWitt, *Fundamentals of Heat and Mass Transfer*, John Wiley & Sons, New York, 1996.
- [31] Y. Wang, C.-Y. Wang, *J. Power Sources* 147 (2005) 148.